

# Ab initio prediction on ferrotoroidic olivine



Hong-Jian Feng , Fa-Min Liu

*Department of Physics, School of Science, Beijing University of Aeronautics and  
Astronautics, Beijing 100083, China*

---

## Abstract

First-principles calculation predict that olivine  $\text{Li}_4\text{MnFeCoNiP}_4\text{O}_{16}$  has ferrotoroidic characteristic and ferrimagnetic configuration with magnetic moment of  $1.56\mu_B$  per formula unit. The ferrotoroidicity of this material makes it a potential candidate for magnetoelectric materials . Based on the orbital-resolved density of states for the transition-metal ions in  $\text{Li}_4\text{MnFeCoNiP}_4\text{O}_{16}$ , the spin configuration for  $\text{Mn}^{2+}$ ,  $\text{Fe}^{3+}$ ,  $\text{Co}^{2+}$ , and  $\text{Ni}^{2+}$  is  $t_{2g}^3(\uparrow)e_g^2(\uparrow)$   $t_{2g}^3(\downarrow)e_g^2(\downarrow)$   $t_{2g}^1(\downarrow)t_{2g}^3(\uparrow)e_g^1(\downarrow)e_g^2(\uparrow)$  and  $t_{2g}^2(\uparrow)t_{2g}^3(\downarrow)e_g^1(\uparrow)e_g^2(\downarrow)$ , respectively. Density functional theory plus U (DFT+U) shows a indirect band gap of 1.25 eV in this predicted material, which is not simply related to the electronic conductivity in terms of being used as cathode material in rechargeable Li-ion batteries.

*Key words:* Ferrotoroidic; Density functional theory; Density of states

*PACS:* 71.15.Mb; 71.20.-b; 75.80.+q

---

## 1 Introduction

Ferrotoroidic(FTO) domains have been observed in olivine  $\text{LiCoPO}_4$  recently using second harmonic generation (SHG), which are independent of the anti-ferromagnetic(AFM) domains [1]. The ordered arrangement of magnetic vortices is found to be the fourth form of ferroic order, which is currently debated whether to be included or not[2,3,4,5,6]. The well-known three forms of ferroic are ferromagnetism, ferroelectricity, and ferroelasticity. This fourth form of ferroic is named as ferrotoroidicity corresponding to the former three forms ,which have been established well and investigated extensively. A ferrotoroidic moment is generated by a vortex of magnetic moment, which is asymmetric under the reversal of time and space. The time- and space- asymmetric property relate ferrotoroidic materials deeply to the multiferroic materials, in which ferromagnetic property violates time reversal symmetry and ferroelectric property violates spatial inversion symmetry. In multiferroic materials, magnetization can be rotated by an external electric field, and polarization can be reversed by a reversal magnetic field, which is called the magnetoelectric effect. Therefore, FTO materials can be used as magnetoelectric materials, in which a magnetization is induced by an electric field, and vice versa, and have potential applications in information storage, the emerging field of spintronic , and sensors.

In olivine  $\text{LiCoPO}_4$ , the  $\text{Co}^{2+}$  ions are located at positions  $(1/4+\epsilon, 1/4, -\delta)$ , where  $\epsilon$  and  $\delta$  represent the small displacements by the  $mmm$  symmetry. The four nearest  $\text{Co}^{2+}$  are arranged antiferromagnetically along the  $y$  axis and have two different toroidic moments due to the rotation of spins by  $\phi = 4.6^\circ$  away from  $y$  axis[7].The two toroidic moments are opposite in direction and

not equal in value, leading to the ferrotoroidic property. Magnetism can be improved by substitution with the transition-metal ions by another one such as in  $\text{Bi}_2\text{FeCrO}_6$ [8] and  $\text{Bi}_2\text{FeTiO}_6$ [9]. In this paper, we put the high-spin  $\text{Mn}^{2+}$  and  $\text{Fe}^{3+}$  in the sites with larger toroidic radius while low-spin  $\text{Co}^{2+}$  and  $\text{Ni}^{2+}$  in the sites with smaller toroidic radius, which would bring about a large resulting toroidic moments and further an excellent ferrotoroidicity. This predicted olivine structural material,  $\text{Li}_4\text{MnFeCoNiP}_4\text{O}_{16}$ , is expected to have significant magnetoelectric effect as multiferroic materials due to ferrotoroidicity, and also have potential to be used as cathode materials for Li-ion rechargeable batteries. In order to gain much insight in this predicted material, we have investigated the electronic and ferrotoroidic properties using first-principles calculations. The remainder of this article is organized as follows: in section 2, we present the computational details of our calculations. In section 3, we report the calculated results and discussion. In section 4, the conclusions based on our calculation are given.

## 2 Computational details

Calculations in this work have been done using the Quantum-ESPRESSO package[10]. Our density functional theory(DFT) computations follow the method previously reported in Ref.[9]. We used our self-interaction-corrected ultrasoft pseudopotential implementation with the Perdew Burke Ernzerhof (PBE) exchange correlation functional, as the common local density approximation(LDA) fails to obtain a band gap in the transition-metal oxides. Plane-wave basis set with kinetic energy cut-off of 38 Ry was employed. Li 2s, Mn 3s, 3p and 3d electrons, Fe 3s, 3p and 3d electrons, Co 3s, 3p and 3d elec-

trons, Ni 3s, 3p and 3d electrons, P 3s and 3p electrons, and O 2s and O 2p electrons have been treated as valence states. We used up to  $6 \times 7 \times 8$  grids of special k points in total energy calculation, and  $8 \times 9 \times 10$  grids of special k points were used for density of states(DOS) calculation. The lattice constants and the atomic positions were taken from Ref.[11] and [12]. Then, fully structural relaxations were performed by minimization of the Hellman-Feynman forces within a convergency threshold of  $10^{-3}$  Ry/Bohr. The transition-metal ions were arranged differently to find the favorable structure with minimal energy. Consequently, the stable structural configuration is obtained and constructed by XCrySDen[13] as in Fig.1, in which the unit cell doubled along the  $b$  axis. Collinear spin configurations have been used to construct the different AFM order. The favorable configuration is obtained as shown in Fig. 2 accordingly. Local density approximation(LDA) or generalized gradient approximation(GGA) within DFT always predicts the conduction properties in transition-metal oxides, and tends to over-delocalize electrons when the kinetic energy of electrons is not large enough to overcome the on-site repulsion. Hence, a Hubbard like term  $U$  is introduced and taken as in Ref.[14] to treat the transition-metal ions, which is named as DFT+ $U$ .

### 3 Results and discussion

It is known that  $\text{LiMPO}_4$  ( $M=\text{Mn, Fe, Co, and Ni}$ ) has an orthorhombic cell, which contains four formula units, 28 atoms: 4 lithium, 4  $M$ , 4 phosphor, and 16 oxygen atoms. Phosphor ions are tetrahedrally coordinated to oxygen, where  $M$  and lithium ions occupy the centers of distorted oxygen octahedral with space group  $Pnma$  as shown in Fig.1. The lattice parameters and atomic

positions are from Ref.[11] and [12], and we put the Mn, Fe, Co, and Ni ions on the  $4M$  sites, respectively. The stable structure under the condition of minimal total energy is shown in Fig. 1. The high-spin  $Mn^{2+}$  and  $Fe^{3+}$  occupy the sites having large toroidic radius, which tends to generate a net toroidic moment as we expected. In Fig. 2, atoms in one unit cell are projected on the XY plane to make clear the relative positions of these four type of ions. Next, the lattice parameters and atomic positions are fully relaxed. The relaxed lattice parameters and Wyckoff positions are shown in Table 1. The lattice parameters are about the averaged values of  $LiMPO_4$  ( $M=Mn, Fe, Co, \text{ and } Ni$ ) due to the mixing of different transition-metal ions.

Let's discuss the magnetic ordering of these four type of ions in the system. The spin configurations are constructed as no spin, ferromagnetic, and four anti-ferromagnetic configurations (denoted as NM, FM, AFM1, AFM2, AFM3 and AFM4, respectively). The AFM configuration are shown in Table 2 in detail, and the four atomic sites to different AFM configuration are Co, Mn, Ni, and Fe as shown in Fig.2 anticlockwise, and the y axis is taken as the positive direction. The differences in the total energy in the NM, AFM1, AFM2, AFM3, and AFM4 configuration relative to its total energy in the FM configuration are shown in Table 2. One can see that the NM configuration has the highest total energy and becomes the most unstable configuration. The AFM2 is the optimum magnetic configuration shown in Fig.2. A resulting magnetic moment of  $1.56 \mu_B$  is obtained from calculation, which is related deeply with the real spin configuration of the four transition-metal elements, which will be discussed in detail in the following sections.

The spin part of the toroidic moment is expressed as

$$\mathbf{T} \propto \sum_n \mathbf{r}_n \times \mathbf{s}_n, \quad (1)$$

where  $\mathbf{r}_n$  is the radius vector and  $\mathbf{s}_n$  is the spin of the  $n$  magnetic ions, and the center of the unit cell is taken as the origin. As we know, the Mn and Fe ions are expected to be in the higher spin states as compared with Co and Ni ions. Therefore, as long as spins rotate away from  $y$  axis, from the favorable structure shown in Fig.2, we get

$$\mathbf{r}_{Mn,Fe,n} \times \mathbf{s}_{Mn,Fe,n} > \mathbf{r}_{Co,Ni,n} \times \mathbf{s}_{Co,Ni,n}. \quad (2)$$

Hence, a large resulting toroidic moment can be obtained in this predicted system as compared with the case in  $\text{LiCoPO}_4$ . From the calculation above, we consider the ferrotoroidic and ferrimagnetic properties can be achieved simultaneously.

The DFT+U method combines the high efficiency of LDA/GGA, and an explicit treatment of correlation with a Hubbard-type model for a subset of states in the system. The total energy is expressed as

$$E_{LDA+U}[n(r)] = E_{LDA}[n(r)] + E_{Hub}[\{n_m^{I\delta}\}] - E_{dc}[\{n^{I\delta}\}], \quad (3)$$

where  $n(r)$  denotes the charge density and  $n^{I\delta}$  is the transition-metal on-site occupation matrix. From the expansion in spherical harmonics, in first order approximation, we have

$$E_{LDA+U} = E_{LDA}[n(r)] + E_U[\{n_{mm'}^{I\delta}\}] = E_{LDA}[\rho] + \frac{U}{2} \sum_{I,\delta} Tr[n^{I\delta}(1 - n^{I\delta})] \quad (4)$$

In present work,  $U$  is 3.92, 3.71, 5.05, and 5.26 for Mn, Fe, Co, and Ni[14], respectively.

The total density of states(DOS) using DFT and DFT+U for  $\text{Li}_4\text{MnFeCoNiP}_4\text{O}_{16}$  are shown in Fig.3, and the DOS of  $\text{LiCOPO}_4$  is also reported for comparison. From the DOS of  $\text{LiCOPO}_4$  and  $\text{Li}_4\text{MnFeCoNiP}_4\text{O}_{16}$ , it is clear that the manifold states near the Fermi level in  $\text{Li}_4\text{MnFeCoNiP}_4\text{O}_{16}$  are attributed to the other transition-metal elements(Mn, Fe, and Ni) except Co. It can be seen that DFT predicts a half-metal behavior, in which there is only a complete spin polarization of electrons at the Fermi level. The strong localization of  $3d$ -electrons of these transition-metal leads to the states passing through the Fermi energy, and further to the half-metal characteristic. The strong correlation of these  $3d$  electrons are well described by employing the DFT+U, and an indirect band gap of  $\sim 1.25$  eV is found in the predicted material.

In Fig.4 we present the DFT+U band structure of  $\text{Li}_4\text{MnFeCoNiP}_4\text{O}_{16}$  for majority spin. It can be seen that it is a semiconductor with an indirect band gap  $\sim 1.25$  eV. The valence band top and conduction band bottom lie, respectively, at S and  $\Gamma$  points of the first Brillouin zone. This suggests that the electronic conduction performance of this new material is not very good. A large band gap will lead to a very small number of intrinsically generated electrons or holes when it is used as the cathode material for Li-ion rechargeable batteries. Therefore, the band gap will not play any significant role in setting the concentration of conduction electrons or holes. It is likely that the key electrons involved in transport in the predicted material are not delocalized electrons, but localized small polarons[15], and polaron mobility is determined by the hopping rate of the polarons. On the other hand, an excellent magnetoelectric effect can be achieved by the insulating property, in which the current leakage is well inhibited. Moreover, from the band dispersion, the valence bands are very dense with little dispersion, while the conduction bands have distinctive

dispersions, and these dispersive conduction bands are well above the Fermi energy.

In order to gain insight in the spin configuration and the oxidation states of the transition-metal elements in the new predicted system, we report the orbital-resolved DOS for Mn, Fe, Co, and Ni in Fig. 5, Fig. 6, Fig. 7, and Fig.8, respectively. From Fig.5 , the majority-spin(up-spin) Mn-3d states in  $d_{xy}$ ,  $d_{yz}$ ,  $d_{z^2}$ ,  $d_{xz}$ , and  $d_{x^2-y^2}$  orbitals are all occupied, and minority-spin(down-spin) in corresponding orbitals are all empty. This result is the formal high-spin(S=5/2) state of  $Mn^{2+}$  with  $t_{2g}^3(\uparrow)e_g^2(\uparrow)$  configuration. Moreover, the majority-spin in  $d_{z^2}$  orbital is pushed away from the Fermi level as compared with the other orbitals, which is partly caused by the specific crystal field. It is worth pointing that all minority-spin are well above the Fermi level.

From Fig. 6, the majority-spin Fe-3d states in  $d_{xy}$ ,  $d_{yz}$ ,  $d_{z^2}$ ,  $d_{xz}$ , and  $d_{x^2-y^2}$  orbitals are all occupied, and minority-spin in corresponding orbitals are all empty. The partial DOS of Fe-3d indicates the high-spin(S=5/2) state of  $Fe^{3+}$  with  $t_{2g}^3(\downarrow)e_g^2(\downarrow)$  configuration. The majority- and minority-spin are all pushed rather away from the Fermi level due to applying the DFT+U, which improves the correlation of 3d-electrons. The minority-spin in  $d_{z^2}$  orbital is far away as in Mn-3d states.

From Fig.7, majority-spin for Co-3d states in all five orbitals are filled, while minority-spin in  $d_{xy}$ ,  $d_{xz}$ , and  $d_{x^2-y^2}$  are partially occupied, and in  $d_{z^2}$  are fully filled, indicating the complicated spin configuration. Based on the partially occupied three orbitals and fully occupied one orbitals in minority-spin states, we regard the Co as the high-spin(S=3/2) state of  $Co^{2+}$  with  $t_{2g}^1(\downarrow)t_{2g}^3(\uparrow)e_g^1(\downarrow)e_g^2(\uparrow)$  configuration.



From Fig. 8, It can be seen the spin configuration for Ni is rather complicated as compared with the other transition-metal elements in the system. Majority- and minority-spin are all filled in Ni-3d states. Majority-spin in  $d_{x^2-y^2}$  and  $d_{xz}$  are near the Fermi level, which is partly caused by the employment of DFT+U, and some of these majority-spin would lie above the Fermi level within DFT. Based on the occupation of all spin states, we consider that Ni is in low-spin(S=2/2) state of Ni<sup>2+</sup> with  $d^8$  configuration. Interestingly, the three majority-spin electrons have possibility to occupy all five orbitals, and this point need to be studied further. This feature would decrease the magnetic moment of Ni<sup>2+</sup>, which is in good agreement with the net magnetic moment of  $1.56 \mu_B$  calculated. Based on the assumption that the majority-spin near Fermi level in  $d_{x^2-y^2}$  and  $d_{xz}$  is derived from the conduction bands within DFT+U, we consider that the spin configuration for Ni<sup>2+</sup> is  $t_{2g}^2(\uparrow)t_{2g}^3(\downarrow)e_g^1(\uparrow)e_g^2(\downarrow)$

Based on the structural analysis and spin configuration, the toroidic moment caused by Mn and Fe is greater than that caused by Co and Ni, which leads to a net toroidic moment and further to ferrotoroidic characteristic, accompanying with a ferrimagnetic configuration. This material can be used as multiferroic material due to its magnetoelectric coupling effect, and possible candidate for cathode material in rechargeable Li-ion batteries. For the latter, the electronic conductivity is not only simply related to the indirect band gap, but also related to localized small polarons and polaron conduction.

## 4 Conclusions

Motivated by the ferrotoroidic domains observed in LiCoPO<sub>4</sub>, we predicted a new material by means of partial substitution of Co by Mn, Fe, and Ni

ions, in which the high-spin Mn and Fe ions are placed on the sites with large toroidic radius. Therefore, this material is expected to have excellent ferrotoroidictiy, and it can be used as multiferroic material in terms of its magnetoelectric effect due to the ferrotoroidicity. The new system also possesses a ferrimagnetic configuration with magnetic moment of  $1.56 \mu_B$ . DFT+U reveal that the indirect band gap is  $\sim 1.25$  eV, the electronic conductivity in  $\text{Li}_4\text{MnFeCoNiP}_4\text{O}_{16}$  is not simply related to the band gap. The valence state is found to be  $\text{Mn}^{2+}$ ,  $\text{Fe}^{3+}$ ,  $\text{Co}^{2+}$ , and  $\text{Ni}^{2+}$  for Mn, Fe, co, and Ni ions, respectively.

### Acknowledgement

The idea for this work was inspired by a talk with Dr. Xiao-Jian Wang.

### References

- [1] B. B. Van Aken, J.-P. Rivera, H. Schmid, M. Fiebig, *Nature* 449 (2007) 702.
- [2] M. Fiebig, *J. Phys. D: Appl. Phys.* 38 (2005) R123.
- [3] V.M.Dubovik, V.V.Tugushev, *Phys. Rep.* 187 (1990) 145.
- [4] A.A.Gorbatsevich, Y.V.Kopaev, *Ferroelectrics* 161 (1994) 321.
- [5] D.G.Sannikov, *Ferroelectrics* 219 (1998) 177.
- [6] H.Schmid, *Ferroelectrics* 252 (2001) 41.
- [7] D.Vaknin, J.L.Zarestky, L.L.Millier, J.-P.Rivera, H.Schid, *Phys. Rev. B* 65 (2002) 224414.
- [8] P. Baettig, N.A.Spaldin, *Appl.Phys.Lett* 86 (2005) 012505.
- [9] H.-J. Feng , F.-M. Liu, *Phys.Lett.A*(2007),doi:10.1016/j.physleta.2007.10.039.
- [10] S.Baroni , A.Dal Corso , S.de Gironcoli , P. Giannozzi , C.Cavazzoni, G. Ballabio, S.Scandolo, G. Chiarotti, P.Focher, A. Pasquarello, K.Laasonen, A.Trave, R.Car, N.Marzari, A.Kokalj<http://www.pwscf.org/>.

- [11] V.A.Streltsov,E.L.Belokoneva,V.G.Tsirelson,N.K.Hansen, Acta Crystallogr., Sect.B: Struct. Sci. 49 (1993) 147.
- [12] F.Kubel,Z.Kristallogr, Mineral. 209 (1994) 755.
- [13] A.Kokalj, J. Mol. Graphics Model. 17 (1999) 176.
- [14] F.Zhou,M.Cococcioni,C.A.Marianetti,D.Morgan,G.Ceder, Phys. Rev. B 70 (2004) 235121.
- [15] T. Maxisch,F. Zhou,G. Ceder, Phys. Rev. B 73 (2006) 104301.

Table 1

Relaxed lattice parameters and wyckoff positions.

$a(\text{\AA})$	$b(\text{\AA})$	$c(\text{\AA})$	$V(\text{\AA})^3$	Wyckoff positions			
10.3324	6.0105	4.6922	291.3992	Li	0.0000	0.0000	0.0000
				Mn	0.7787	0.2500	0.5210
				Fe	0.2213	0.7500	0.4790
				Co	0.2787	0.2500	0.9790
				Ni	0.7213	0.7500	0.0210
				P	0.0964	0.2500	0.4218
				O1	0.0997	0.2500	0.7476
				O2	0.4546	0.2500	0.2019
				O3	0.1704	0.0415	0.2804

Table 2

AFM magnetic configuration and calculated differences in total energy ( $\Delta E$ ) in the NM, AFM1, AFM2, AFM3, and AFM4 configuration relative to its total energy in the FM configuration in units of eV/formular unit. The four atomic sites to different AFM configuration are Co, Mn, Ni, and Fe anticlockwise. The y axis is set as the positive direction.

	AFM1	AFM2	AFM3	AFM4	NM
magnetic configuration	$\uparrow\uparrow\downarrow\downarrow$	$\uparrow\downarrow\uparrow\downarrow$	$\downarrow\downarrow\uparrow\uparrow$	$\downarrow\uparrow\downarrow\uparrow$	
$\Delta E$	-0.02	-0.08	-0.05	-0.07	1.35

### Figure captions:

Fig.1 Crystal structure of  $\text{Li}_4\text{MnFeCoNiP}_4\text{O}_{16}$  showing two unit cells constructed by XCrySDen(Ref.[13]).

Fig.2 The favorable antiferromagnetic configuration projected onto the XY plane. The length of the arrow indicates the strength of magnetism

Fig. 3 Total DOS of  $\text{Li}_4\text{MnFeCoNiP}_4\text{O}_{16}$  within (a)DFT+U ,and(b) DFT. (c) show the DOS of  $\text{LiCoPO}_4$  within DFT+U.

Fig.4 Electronic band structure of  $\text{Li}_4\text{MnFeCoNiP}_4\text{O}_{16}$  for the majority-spin states. The dotted line indicates the Fermi energy.

Fig. 5 Orbital-resolved DOS for Mn in  $\text{Li}_4\text{MnFeCoNiP}_4\text{O}_{16}$ . (a), (b), (c), (d), and (e) show the DOS for  $d_{xy}$ ,  $d_{yz}$ ,  $d_{z^2}$ ,  $d_{xz}$ , and  $d_{x^2-y^2}$  orbitals respectively. Majority-spin states are shown in the upper portions and minority-spin states in the lower portions in all panels. The Fermi level is set to zero.

Fig. 6 Orbital-resolved DOS for Fe in  $\text{Li}_4\text{MnFeCoNiP}_4\text{O}_{16}$ . (a), (b), (c), (d), and (e) show the DOS for  $d_{xy}$ ,  $d_{yz}$ ,  $d_{z^2}$ ,  $d_{xz}$ , and  $d_{x^2-y^2}$  orbitals respectively. Majority-spin states are shown in the upper portions and minority-spin states in the lower portions in all panels. The Fermi level is set to zero.

Fig. 7 Orbital-resolved DOS for Co in  $\text{Li}_4\text{MnFeCoNiP}_4\text{O}_{16}$ . (a), (b), (c), (d), and (e) show the DOS for  $d_{xy}$ ,  $d_{yz}$ ,  $d_{z^2}$ ,  $d_{xz}$ , and  $d_{x^2-y^2}$  orbitals respectively. Majority-spin states are shown in the upper portions and minority-spin states in the lower portions in all panels. The Fermi level is set to zero.

Fig. 8 Orbital-resolved DOS for Ni in  $\text{Li}_4\text{MnFeCoNiP}_4\text{O}_{16}$ . (a), (b), (c), (d), and (e) show the DOS for  $d_{xy}$ ,  $d_{yz}$ ,  $d_{z^2}$ ,  $d_{xz}$ , and  $d_{x^2-y^2}$  orbitals respectively.

Majority-spin states are shown in the upper portions and minority-spin states in the lower portions in all panels. The Fermi level is set to zero.

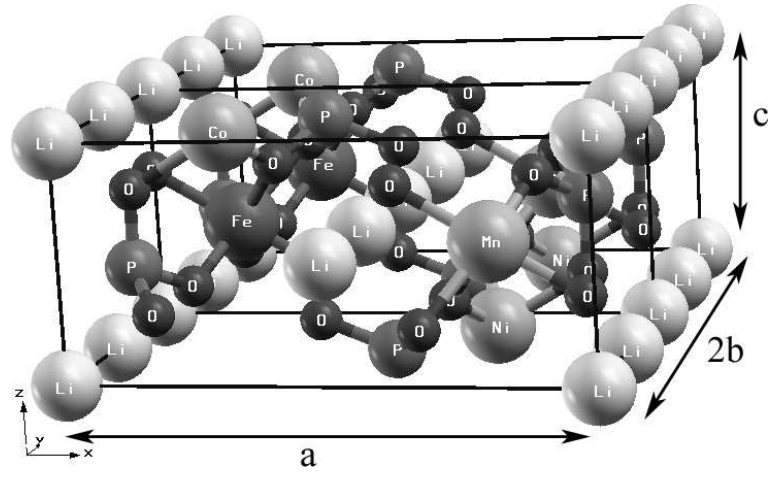


Fig. 1. Crystal structure of  $\text{Li}_4\text{MnFeCoNiP}_4\text{O}_{16}$  showing two unit cells constructed by XCrySDen(Ref.[13]).

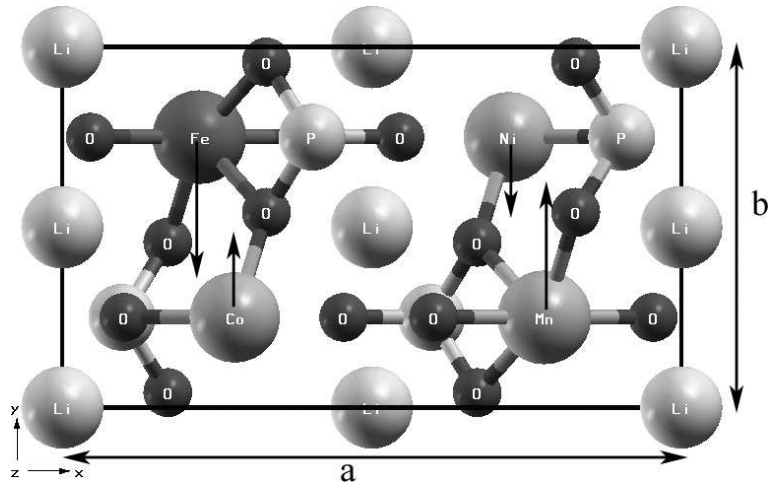


Fig. 2. The favorable antiferromagnetic configuration projected onto the XY plane. The length of the arrow indicates the strength of magnetism.

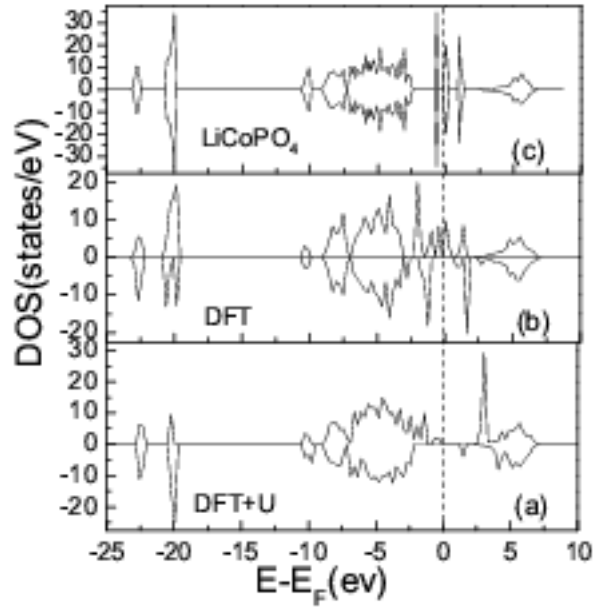


Fig. 3. Total DOS of  $\text{Li}_4\text{MnFeCoNiP}_4\text{O}_{16}$  within (a)DFT+U , and(b) DFT. (c) show the DOS of  $\text{LiCoPO}_4$  within DFT+U.

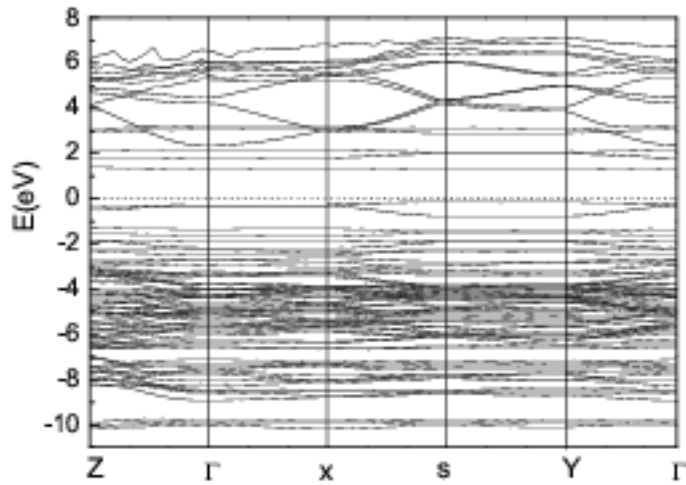


Fig. 4. Electronic band structure of  $\text{Li}_4\text{MnFeCoNiP}_4\text{O}_{16}$  for the majority spin states. The dotted line indicates the Fermi energy.



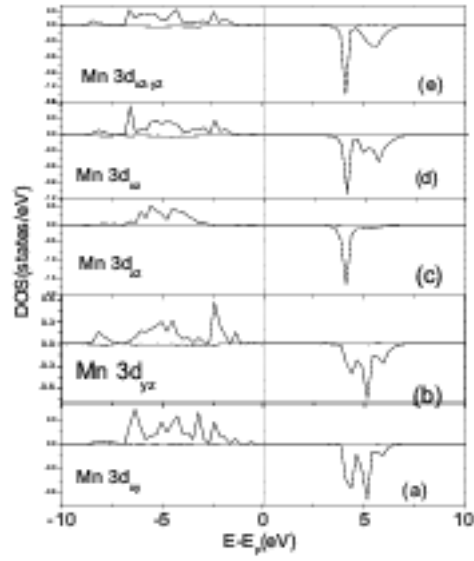


Fig. 5. Orbital-resolved DOS for Mn in  $\text{Li}_4\text{MnFeCoNiP}_4\text{O}_{16}$ . (a), (b), (c), (d), and (e) show the DOS for  $d_{xy}$ ,  $d_{yz}$ ,  $d_{z^2}$ ,  $d_{xz}$ , and  $d_{x^2-y^2}$  orbitals respectively. Majority-spin states are shown in the upper portions and minority-spin states in the lower portions in all panels. The Fermi level is set to zero.

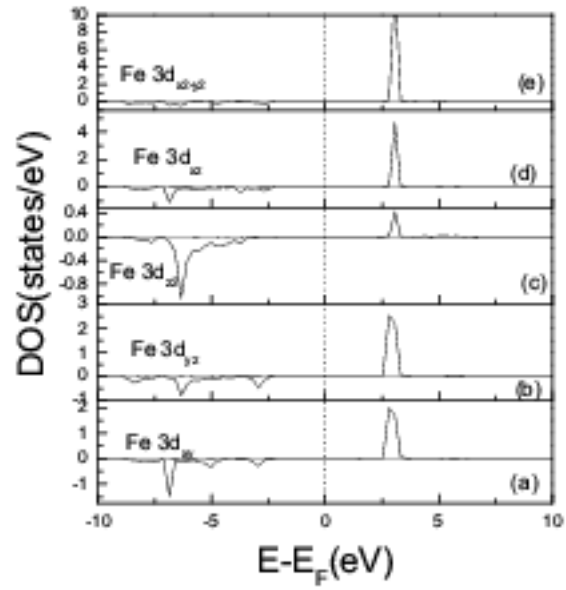


Fig. 6. Orbital-resolved DOS for Fe in  $\text{Li}_4\text{MnFeCoNiP}_4\text{O}_{16}$ . (a), (b), (c), (d), and (e) show the DOS for  $d_{xy}$ ,  $d_{yz}$ ,  $d_{z^2}$ ,  $d_{xz}$ , and  $d_{x^2-y^2}$  orbitals respectively. Majority-spin states are shown in the upper portions and minority-spin states in the lower portions in all panels. The Fermi level is set to zero.

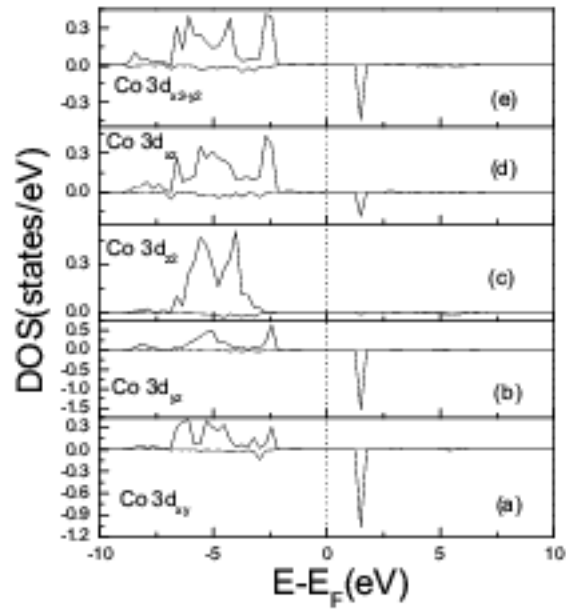


Fig. 7. Orbital-resolved DOS for Co in  $\text{Li}_4\text{MnFeCoNiP}_4\text{O}_{16}$ . (a), (b), (c), (d), and (e) show the DOS for  $d_{xy}$ ,  $d_{yz}$ ,  $d_{z^2}$ ,  $d_{xz}$ , and  $d_{x^2-y^2}$  orbitals respectively. Majority-spin states are shown in the upper portions and minority-spin states in the lower portions in all panels. The Fermi level is set to zero.

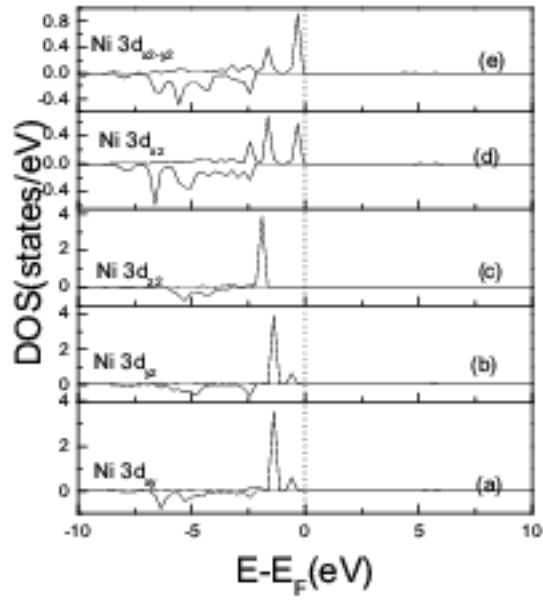


Fig. 8. Orbital-resolved DOS for Ni in  $\text{Li}_4\text{MnFeCoNiP}_4\text{O}_{16}$ . (a), (b), (c), (d), and (e) show the DOS for  $d_{xy}$ ,  $d_{yz}$ ,  $d_{z^2}$ ,  $d_{xz}$ , and  $d_{x^2-y^2}$  orbitals respectively. Majority-spin states are shown in the upper portions and minority-spin states in the lower portions in all panels. The Fermi level is set to zero.